Quad-Active-Bridge Converter With Current Balancing Coupled Inductor for SST Application

Nabeel Naseem, *Student Member, IEEE*, and Honnyong Cha, *Senior Member, IEEE*

***Abstract*—In this article, a current balancing coupled inductor (CBCL) based asymmetrically configured quad-active-bridge (QAB) converter is proposed. The QAB converter provides high-frequency isolation for a dc–dc stage of a solid state transformer (SST), as well as provides a modular solution to the SST medium-voltage (MV) dc link. The proposed CBCL ensures current balancing among/three active H-bridges without using any dedicated controller and without expensive sensors when transferring equal power from MV to low-voltage side. The proposed CBCL is the integration of three inductors of the active H-bridges required for power transfer and zero-voltage-switching and does not require an extra magnetic volume. Experimental results are presented to validate the performance.**

***Index Terms*—CBCL, current balance, current balancing coupled inductor (CBCL), imbalanced current, QAB converter, quad-active-bridge (QAB), solid-state-transformer (SST).**

NOMENCLATURE

i and j	Subindex indicating to which active H-bridge $\{A, B, C, D\}$ the element belongs.
$i_{Li}(t)$	Current of inductor connected to active H-bridge i.
$v_{oi}(t)$	Rectangular ac voltage of active H-bridge i.
$v_{oi}{}'(t)$	Reflected equivalent rectangular ac voltage of active H-bridge i.
V_{dci}	DC voltage connected to active H-bridge i.
φ_i	Phase angle of $v_{oi}(t)$ in radians.
φ_{ij}	Phase difference between the rectangular ac voltage of active H-bridges i and j.
P_{ij}	Power flow between active H-bridges i and j.
f_s	Switching frequency.
x	Point of common coupling among the four rectangular ac voltage sources.
$v_x(t)$	Voltage of the point of common coupling.
n_i	Number of turns associated with isolated HF transformer winding connected to active H-bridge i.
$n_{\rm MV}$, $n_{\rm LV}$	Number of turns of isolated HF transformer winding connected to MV and LV side active H-bridges, respectively.
n	Turns ratio of $n_{\rm MV}$ and $n_{\rm LV}$.
L_e	Equivalent inductance.
L_i	ZVS or power transfer inductance connected to active H-bridge i.
$\psi_A,\ \psi_B,\ \psi_C$	Magnetic fluxes generated in three outer legs of the proposed CBCL.
$L_{{\rm Self}A},\ L_{{\rm Self}B},$ $L_{{\rm Self}C}$	Self-inductances of the proposed CBCL.
$L_{{\rm lk}A},\ L_{{\rm lk}B},\ L_{{\rm lk}C}$	Leakage inductances of the proposed CBCL.
$M_{AB},\ M_{BC},\ M_{CA}$	Mutual inductances between the windings of the proposed CBCL.
$k_{AB},\ k_{BC},\ k_{CA}$	Coupling coefficients between the windings of the proposed CBCL.
$\mathcal{R}_c$, r, $\mathcal{R}_{\rm g}$	Magnetic reluctances of the UU-shaped ferrite cores along the magnetic path length, perpendicular to magnetic path length, and the air gap, respectively.
$\psi_1,\ \psi_2,\ \psi_3$	Window fluxes illustrated in the reluctance model of the proposed CBCL.
$\psi_{\rm net}$	Net generated flux in the proposed CBCL due to unbalanced currents.
$v_A,\ v_B,\ v_C$	Voltage across the winding of the proposed CBCL.

Manuscript received August 13, 2020; revised November 13, 2020, January 19, 2021, and March 18, 2021; accepted April 13, 2021. Date of publication April 29, 2021; date of current version July 30, 2021. This work was supported by the National Research Foundation of Korea grant funded by the Korea government (MSIT) (NRF-2021R1A2C2007879). This paper was presented in part at the 10th International Conference on Power Electronics and ECCE Asia, Busan, South Korea, 2019. Recommended for publication by Associate Editor Z. Li. (*Corresponding author: Honnyong Cha.*)

The authors are with the School of Energy Engineering, Kyungpook National University, Daegu 702-701, South Korea (e-mail: nabeelnaseem@gmail.com; chahonny@knu.ac.kr).

Color versions of one or more figures in this article are available at https://doi.org/10.1109/TPEL.2021.3076460.

Digital Object Identifier 10.1109/TPEL.2021.3076460

I. INTRODUCTION

BECAUSE of the increasing growth in the load, the penetration of renewables, and deployment of the distributed generation at the consumer end, smart grid has drawn the attention of the researchers and industry as a viable solution to the existing electrical system. The power electronics based transformer or solid state transformer (SST) is one of the key advancements in the distribution system. An SST increases the reliability of the distribution system by providing multiple

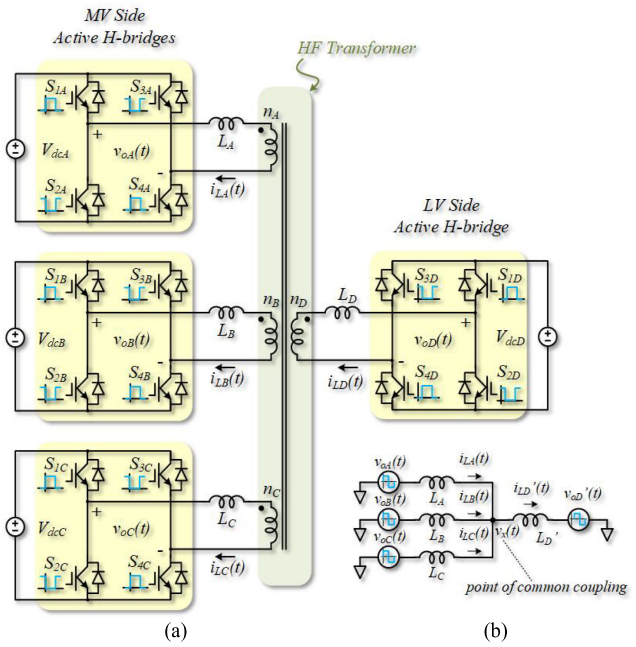

Fig. 1. (a) Conventional asymmetric configuration of a QAB converter using separate uncoupled ZVS inductors. (b) Equivalent circuit diagram.

ports for the distributed energy resources and distributed energy storage. The SST-based microgrid integrates the high-frequency (HF) transformer, rectifier, dc–dc, and ac–dc converters in a single module. The SST with HF isolation provides several advantages such as fault isolation, dc output, voltage sag, outage compensation, and harmonic isolation, and can supply stable and clean power for dc distribution with high efficiency, reliability, and maneuverability [1].

Different topologies have been proposed for SST dc–dc stage. Two solutions have been investigated widely: 1) single converter with high-voltage and high current rating devices, and 2) a modular solution, to share voltage and power among the constituent modules using low-voltage (LV), low current rating devices [2]. The quad-active-bridge (QAB) converter has received more attention as a single converter module for a LV dc system, as well as a modular solution to the SST HF isolated dc–dc stage [3], [4]. Compared to a dual-active-bridge (DAB) converter, the number of transformers is reduced to one-third. The QAB converter has a single magnetic link which allows direct power exchange among four active H-bridges connected to a single four winding transformer [2]. An asymmetrical configuration of the QAB converter has the best optimum tradeoff between cost and efficiency [3], [4]. In this configuration, three active H-bridges are connected to the medium-voltage (MV) side, and one active H-bridge is connected to the LV side. Fig. 1 presented in [22] has shown the architecture of SST employing the asymmetrically configured QAB converter as a solution for the dc–dc stage [2]. In a standard operation scheme, the active H-bridges of MV side process the same amount of power [6], [7]. Transferring equal power between MV and LV side active H-bridges so that all active H-bridges of MV side share equal power is a challenging task. Because it needs a perfect match of circuit parameters between active H-bridges, including of parasitic and leakage inductances of HF transformer connected to MV side [5], [8]. It is observed that the MV side active H-bridges of asymmetrically configured QAB converter does not share equal power and causes unequal switch stresses and unequal heat dissipation. The condition becomes worst when the power increases to maximum ratings. There may be several causes of the mismatch in circuit parameters, some of them includes mismatch in gate signal generation, unequal propagation delay in gate drivers, mismatch in switch on resistance/voltages, mismatch in zero-voltage-switching (ZVS) or leakage inductances, uneven parasitic elements in HF transformer, unequal dc voltages, and unequal phase-shift angles between simultaneous active H-bridges. Mass production of such converters for SST applications in the future may have some tolerances and mismatches in circuit parameters. Moreover, a perfect match of circuit parameters is impractical.

An aforementioned problem caused by tolerances in circuit parameters has been addressed extensively [9]–[13]. A *dq*-model based control strategy has been proposed to balance the voltage and power through parallel DAB modules of an SST [12]. The QAB converter requires an additional control loop to equalize the power of the MV side active H-bridges, thus the control effort for implementation is higher [4], [13]. The closed-loop control that controls the power flow as well as the current balancing needs to sense individual currents for feedback control and requires extra control circuitry and expensive sensors for individual current balancing. The QAB converter-based SST structure has multiple active H-bridges on MV side. Therefore, an increased number of expensive sensors and individual current balancing feedback controls make the system expensive, complicated, hard to implement, and less attractive for practical use.

Different magnetic-based strategies have been reported in [14]–[19]. Such methods require fewer components, are less complex and have no stability issues compared to control strategies. Other strategies [15], [17] are intended for two equal current sharing. However, two or more such structures are required for equal sharing of three QAB currents in addition to existing magnetics. Dou *et al.* [17], Noah *et al.* [18], and Zhang *et al.* [19] used customized magnetic cores that are not commercially available which increases the cost. The existing coupled magnetic structures for automatic current balancing do not provide controlled paths for leakage fluxes through the core, and actually provide leakages that are dependent on physical orientation, the spacing of the windings, and parasitic, which can only be changed or increased in a limited range [14]–[19]. Therefore, they need extra additional inductors for ZVS operation that increase the component count and magnetic volume of a converter.

In order to ensure current balancing and generate sufficient inductances without increasing the component count and magnetic volume, a reliable magnetic integration based solution is presented for the QAB converter [20]–[22]. The main contribution of this article is to balance the three currents effectively by physically joining the three existing ZVS inductors together without increasing the magnetic volume of a QAB converter, changing the circuit inductances, using a dedicated

controller, and expensive sensors. A new core structure for the proposed current balancing coupled inductor (CBCL), based on a commercially available U-shaped ferrite core is introduced to distinguish the effect of magnetic coupling and decoupling. This new magnetic structure makes the design simple and intuitive.

II. Asymmetrically Configured QAB Converter

The conventional circuit shown in Fig. 1(a) is an asymmetric configuration of a QAB converter. It consists of three active H-bridges (A, B, and C) on MV side, one active H-bridge D on LV side, an HF transformer with four isolated windings. Separate inductors (L_A, L_B, L_C, and L_D) are connected to each active H-bridge [2]. Power transfer and ZVS operation is achieved with the help of these inductors [11]. With equal specific inductance values, it is hard to integrate these inductors inside the main HF transformer; this complicates the design [8]. The elements of the active H-bridges have subindex $i = \{A, B, C, D\}$ to indicate the active H-bridge the element belongs to. Each active H-bridge i has a dc voltage $V_{\mathrm{dc}i}$ on dc side, inductor current $i_{Li}(t)$, rectangular ac voltage $v_{oi}(t)$ on ac side, at phase φ_i in radians. The ac output of each active H-bridge is connected to HF transformer isolated winding having a number of turns n_i.

Bidirectional power is transferred between MV and LV sides by creating a phase-shift between them. Active H-bridges of MV side are required to share equal power transfer. Assuming that all windings of HF transformer connected to MV side have an equal number of turns $n_{\mathrm{MV}} = n_A = n_B = n_C$, while LV side has a number of turns $n_{\mathrm{LV}} = n_D$. The ratio of n_{MV} to n_{LV} is n. For the ease of understanding, the active H-bridges of MV side can be replaced by equivalent rectangular ac voltage sources $v_{oA}(t)$, $v_{oB}(t)$, and $v_{oC}(t)$. Similarly, active H-bridge D on the LV side can be replaced by a reflected equivalent rectangular ac voltage source $v_{oD}{}'(t)$ on MV side of the HF transformer. The equivalent circuit diagram of the conventional asymmetrical configuration of a QAB converter is shown in Fig. 1(b). The central point x is the point of common coupling among the four rectangular ac voltage sources. The voltage $v_x(t)$ is given as

$$v_x\ (t) = \frac{v_{oA}\,(t) + v_{oB}\,(t) + v_{oC}\,(t) + v'_{oD}\,(t)}{4}. \tag{1}$$

The power flow P_{ij} between any two active H-bridges i and j depends on the phase difference φ_{ij} between them, and generally, expressed as

$$P_{ij} = \frac{nV_{\mathrm{dc}i}V_{\mathrm{dc}j}}{2\pi f_s L_e}\varphi_{ij}\left(1 - \frac{|\varphi_{ij}|}{\pi}\right) \tag{2}$$

$$\varphi_{ij} = \varphi_i - \varphi_j \tag{3}$$

where f_s is switching frequency, $i = \{A, B, C, D\}$, $j = \{A, B, C, D\}$, and L_e is an equivalent inductance seen from MV side and can be equated as

$$L_e = \left(\frac{L_A + L_B + L_C}{3}\right) + n^2 L_D. \tag{4}$$

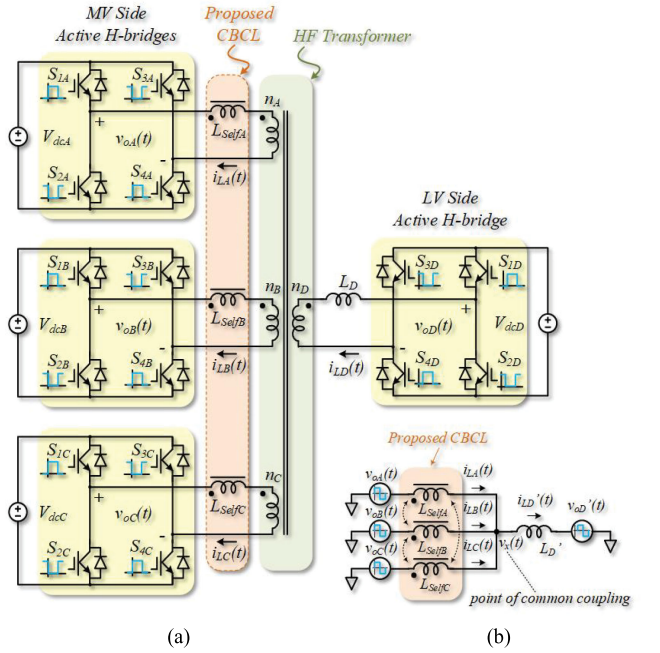

Fig. 2. (a) Proposed asymmetric configuration of a QAB converter using the proposed CBCL instead of separate inductors. (b) Equivalent circuit diagram.

III. Proposed Structure for QAB Converter

The inductors of the conventional structure (see Fig. 1) are integrated to make a single proposed three-winding CBCL. The proposed structure for an asymmetric configuration of a QAB converter using the three-winding CBCL is presented in Fig. 2(a) and its equivalent circuit in Fig. 2(b), respectively. This structure has the proposed CBCL connected to three active H-bridges on the MV side instead of independent separate inductors. No extra magnetic volume is required for the proposed CBCL, and the three independent inductors connected in the conventional structure can be joined together to make a proposed CBCL. This proposed three-winding magnetic integration method can effectively balance the currents in an asymmetrically configured QAB converter and can offer sufficient inductances as well, which are required for power transfer and ZVS operation in each active H-bridge simultaneously. The equivalent inductance seen from the MV side in (4) is now modified as

$$L_e = \left(\frac{L_{\mathrm{lk}A} + L_{\mathrm{lk}B} + L_{\mathrm{lk}C}}{3}\right) + n^2 L_D \tag{5}$$

where $L_{\mathrm{lk}A}$, $L_{\mathrm{lk}B}$, and $L_{\mathrm{lk}C}$ are the leakage inductances of the proposed CBCL.

IV. Proposed Three-Winding CBCL

The key features of the proposed CBCL are as follows.

1) With significant mismatch in circuit parameters, it perfectly balances three individual currents; no separate current balancing transformers are required.

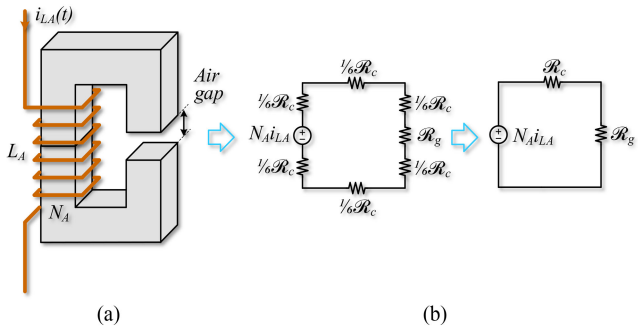

Fig. 3. Separate uncoupled inductor using two U-shaped ferrite cores employed in conventional asymmetric QAB converter. (a) Magnetic structure. (b) Simplified reluctance model.

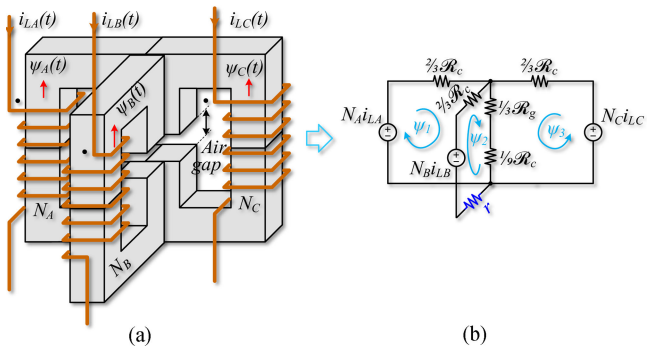

Fig. 4. Proposed CBCL structure using six U-shaped ferrite cores. (a) Magnetic structure. (b) Derived simplified reluctance model.

2) It offers three sufficiently large leakage inductances for ZVS operation as compared to conventional coupled inductors; no extra inductors are needed.
3) It gives the leakage inductances equivalent to the separately designed inductors, so that the circuit inductance does not change [see (14) and (28)].
4) It provides paths for leakage fluxes, which give the controllable leakage inductances that can be varied directly by an air gap as the inductance value of the separate inductors can be controlled simply by the air gap.
5) It does not increase the magnetic volume of a converter because existing ZVS inductors in a conventional QAB converter are used to make the proposed CBCL. No extra magnetics is added to the converter and no more expensive sensors are needed.
6) It saves the cost of current balancing.
7) Design is simple and intuitive, and commercially available magnetic ferrite cores can be used.
8) An air gap in the central legs of the proposed CBCL makes the structure mechanically stable compared to structures that have an air gap in outer legs. Outer legs and windings covering around the air gap produce less electromagnetic interference emission.

These all are achieved by using the new magnetic core structure of the proposed CBCL, which makes it unique compared to other conventional coupled inductors.

A. Magnetic Structure

A commercially available U-shaped ferrite core with an air gap in one leg is chosen for this purpose. It is easily available and made by some manufacturers like Ferroxcube (U46/40/28-3C90) offers different air gaps in one leg on request. The specifications of the magnetic core used in this article are listed in the Appendix. Fig. 3(a) shows the separate uncoupled inductor using two commercially available U-shaped ferrite core with an air gap in one leg. Three such separate uncoupled inductors are joined to integrate the already existing magnetics and make the proposed CBCL as drawn in Fig. 4(a). It has three outer legs and three inner legs. The winding on each outer leg has the number of turns (N_A, N_B, and N_C). The three outer legs provide strong magnetic coupling between the three windings to effectively balance the three currents. The three inner legs with air gaps in the central part of the proposed CBCL provide leakage flux paths for the three windings to generate sufficient leakage inductances. These leakage inductances are used for power transfer and ZVS operation in the QAB converter. Therefore, no extra magnetic volume is required for power transfer and ZVS inductors. The proposed CBCL is used for both purposes.

This integration method results in a nonsymmetric magnetic structure (T-structure) as seen from the top of the structure in Fig. 4(a). The inductors *A* and *C* are joined at an angle of 180° and the inductor *B* is placed perpendicular to inductor *A* and *C* making an angle of 90°. The magnetic flux loops of inductors *A* and *C* are similar to each other, whereas the magnetic flux loop of inductor B is not similar to that of A and C. The magnetic loop of inductor *B* has very small magnetic core reluctance r in series, which makes this loop different from others. This small core reluctance (such that $r \ll \mathcal{R}_c$) is equivalent to the magnetic core reluctance in the direction perpendicular to the magnetic path length of inductors *A* and *C* as shown in Fig. 4(b). Although this integration method results in a nonsymmetric magnetic structure, however, even the nonsymmetric magnetic structure of the proposed CBCL does not affect the balancing performance. The performance validation of the proposed CBCL has been presented in Section V. The governing equations of the proposed three-winding CBCL are summarized as follows:

$$\begin{bmatrix} +L_{\text{Self}A} & -M_{AB} & -M_{AC} \\ -M_{BA} & +L_{\text{Self}B} & -M_{BC} \\ -M_{CA} & -M_{CB} & +L_{\text{Self}C} \end{bmatrix} \begin{bmatrix} \frac{di_{LA}}{dt} \\ \frac{di_{LB}}{dt} \\ \frac{di_{LC}}{dt} \end{bmatrix} = \begin{bmatrix} N_A \frac{d\psi_A}{dt} \\ N_B \frac{d\psi_B}{dt} \\ N_C \frac{d\psi_C}{dt} \end{bmatrix} \tag{6}$$

$$M_{AB} = M_{BA} = k_{AB} \sqrt{L_{\text{Self}A} L_{\text{Self}B}} \tag{7}$$

$$M_{AC} = M_{CA} = k_{CA} \sqrt{L_{\text{Self}A} L_{\text{Self}C}} \tag{8}$$

$$M_{BC} = M_{CB} = k_{BC} \sqrt{L_{\text{Self}B} L_{\text{Self}C}} \tag{9}$$

$$L_{\text{lk}A} = L_{\text{Self}A} - M_{AB} - M_{AC} \tag{10}$$

$$L_{\mathrm{lk}B} = L_{\mathrm{Self}B} - M_{AB} - M_{BC} \tag{11}$$

$$L_{\mathrm{lk}C} = L_{\mathrm{Self}C} - M_{BC} - M_{AC} \tag{12}$$

where ψ_A, ψ_B, and ψ_C are the generated magnetic fluxes, $L_{\mathrm{Self}A}$, $L_{\mathrm{Self}B}$, and $L_{\mathrm{Self}C}$ are the self-inductances of the three windings of the proposed CBCL, respectively, M_{AB}, M_{AC}, and M_{BC} are the mutual inductances; and k_{AB}, k_{BC}, and k_{CA} are the coupling coefficients between the windings of the proposed CBCL. Negative signs with the mutual inductances in (6) represent inverse coupling. To share equal current, the following condition must be fulfilled:

$$N_A = N_B = N_C = N. \tag{13}$$

B. Reluctance Model

Considering $\mathcal{R}_{\mathrm{g}}$ be the magnetic reluctance of the air gap and $\mathcal{R}_c$ as the magnetic core reluctance of two commercially available U-shaped ferrite cores with the assumption that each side of a single U-shaped ferrite core has $(1/6)\mathcal{R}_c$ core reluctance as shown in Fig. 3(b). As the air gap reluctance is much greater than the magnetic core reluctance so the inductance of the conventional separate single inductor without considering the fringing effect can be given as

$$L = \frac{N^2}{\mathcal{R}_{\mathrm{g}}} = \frac{\mu_o N^2 A_c}{l_{\mathrm{g}}} \tag{14}$$

where μ_o is the magnetic permeability of free space, N is the number of turns, A_c is the cross-sectional area of the magnetic core, and l_{g} is the length of the air gap. Joining three such separate models, the simplified reluctance model of the proposed CBCL can be derived as presented in Fig. 4(b). The mesh equations for three window fluxes (ψ_1, ψ_2, ψ_3) can be written as

$$\begin{bmatrix} Ni_{LA} \\ Ni_{LB} \\ Ni_{LC} \end{bmatrix} = \begin{bmatrix} \frac{7}{9}\mathcal{R}_c + \frac{1}{3}\mathcal{R}_{\mathrm{g}} & \frac{1}{9}\mathcal{R}_c + \frac{1}{3}\mathcal{R}_{\mathrm{g}} & \frac{1}{9}\mathcal{R}_c + \frac{1}{3}\mathcal{R}_{\mathrm{g}} \\ \frac{1}{9}\mathcal{R}_c + \frac{1}{3}\mathcal{R}_{\mathrm{g}} & \frac{7}{9}\mathcal{R}_c + \frac{1}{3}\mathcal{R}_{\mathrm{g}} + r & \frac{1}{9}\mathcal{R}_c + \frac{1}{3}\mathcal{R}_{\mathrm{g}} \\ \frac{1}{9}\mathcal{R}_c + \frac{1}{3}\mathcal{R}_{\mathrm{g}} & \frac{1}{9}\mathcal{R}_c + \frac{1}{3}\mathcal{R}_{\mathrm{g}} & \frac{7}{9}\mathcal{R}_c + \frac{1}{3}\mathcal{R}_{\mathrm{g}} \end{bmatrix} \times \begin{bmatrix} \psi_1 \\ \psi_2 \\ \psi_3 \end{bmatrix}. \tag{15}$$

where r is the magnetic core reluctance in the direction perpendicular to the magnetic path length of inductors *A* and *C* as shown in Fig. 4(b). All three magnetic loops have a high air gap reluctance $\mathcal{R}_{\mathrm{g}}$ in addition to low core reluctance $\mathcal{R}_{\mathrm{c}}$. In any inversely coupled inductor, the working inductances are the leakage inductances, which play a role in circuit operation instead of the self-inductances. In the proposed CBCL, $\mathcal{R}_{\mathrm{g}}$ is responsible for leakage inductance and its value is much higher as compared to $\mathcal{R}_{\mathrm{c}}$ and r (such that $\mathcal{R}_{\mathrm{g}} \gg \mathcal{R}_{\mathrm{c}} \gg r$). The effect of r as compared to $\mathcal{R}_{\mathrm{g}}$ in the flux loop can be definitely ignored ($r \approx 0$). Besides, the physical angles of the outer core legs from the central axis of the proposed CBCL do not affect the magnetic flux inside the core significantly. In other words, the leakage inductances of the proposed CBCL are much more sensitive to air gaps as compared to mismatches due to nonsymmetric magnetic structure. Therefore, for ease of analysis, this nonsymmetric magnetic structure (T-structure) can be approximated to a symmetric magnetic structure by assuming the following equations:

$$L_{\mathrm{Self}A} = L_{\mathrm{Self}B} = L_{\mathrm{Self}C} = L_{\mathrm{self}} \tag{16}$$

$$M_{AB} = M_{AC} = M_{BC} = M \tag{17}$$

$$k_{AB} = k_{AC} = k_{BC} = k \tag{18}$$

$$L_{\mathrm{lk}A} = L_{\mathrm{lk}B} = L_{\mathrm{lk}C} = L_{\mathrm{lk}} \tag{19}$$

where L_{self} is the self-inductance of each winding of the proposed CBCL, and M and k are the mutual inductance and magnetic coupling between the windings, respectively. The leakage inductance L_{lk} and self-inductance can now be related as

$$L_{\mathrm{lk}} = L_{\mathrm{Self}}\,(1 - 2k)\,. \tag{20}$$

The window fluxes are the same fluxes generated by the three windings. By solving (15), the window fluxes can be calculated as given in (21) to (23) at the bottom of the next page. Taking the time derivative of window fluxes and multiplying by number of turns, (24) is obtained and shown at the bottom of the next page. Where (v_A, v_B, v_C) are the voltages across the windings of the proposed CBCL. Comparing (6) with (24), the self and mutual inductances of the proposed CBCL are found as

$$L_{Self} = \frac{(4\mathcal{R}_c + 3\mathcal{R}_{\mathrm{g}})}{3\mathcal{R}_c\,(\mathcal{R}_c + \mathcal{R}_{\mathrm{g}})}\,N^2 \tag{25}$$

$$M = \frac{(\mathcal{R}_c + 3\mathcal{R}_{\mathrm{g}})}{6\mathcal{R}_c\,(\mathcal{R}_c + \mathcal{R}_{\mathrm{g}})}\,N^2. \tag{26}$$

By substituting (25) and (26) in (10), the leakage inductance of the proposed CBCL can be determined as

$$\begin{aligned} L_{\mathrm{lk}} &= \frac{(4\mathcal{R}_c + 3\mathcal{R}_{\mathrm{g}})}{3\mathcal{R}_c\,(\mathcal{R}_c + \mathcal{R}_{\mathrm{g}})}\,N^2 - 2\frac{(\mathcal{R}_c + 3\mathcal{R}_{\mathrm{g}})}{6\mathcal{R}_c\,(\mathcal{R}_c + \mathcal{R}_{\mathrm{g}})}N^2 \\ &= \frac{1}{\mathcal{R}_c + \mathcal{R}_{\mathrm{g}}}\,N^2. \end{aligned} \tag{27}$$

As, $\mathcal{R}_{\mathrm{g}} \gg \mathcal{R}_{\mathrm{c}}$

$$L_{\mathrm{lk}} = \frac{N^2}{\mathcal{R}_{\mathrm{g}}}. \tag{28}$$

From (14) and (28), it is found that the leakage inductance of the proposed CBCL is similar to the inductance of the conventional separate uncoupled inductor. Thus, the conventional inductors designed on said cores can easily be joined together without bothering with the leakages and hence current balancing performance is achieved.

C. Magnetic Coupling

A structure used to balance two currents has two isolated windings (Fig. 8, [21]). The flux generated by one winding interacts with that of another winding, so the maximum coupling coefficient, in this case, is 100%. Whereas, a structure used to balance three currents has three isolated windings as shown in Fig. 4(a). The flux generated by each winding interacts

with those of the other two windings; therefore, the maximum coupling coefficient is 50%. However, this is the maximum theoretical value and cannot be achievable in practical designs. Leakage paths in the central part of the proposed CBCL make the coupling coefficient less than 50%. These leakage fluxes are required to generate leakage inductances in the proposed CBCL for power transfer and ZVS operation in the QAB converter. By substituting (25) and (26) in (7), the coupling coefficient between the windings of the proposed CBCL is given as

$$k = \frac{\mathcal{R}_c + 3\mathcal{R}_g}{8\mathcal{R}_c + 6\mathcal{R}_g} \quad (1/8 < k < 1/2). \tag{29}$$

The coupling coefficient of the proposed CBCL is the function of reluctance ratio.

D. Leakage Inductances of Proposed CBCL vs Separate Inductors

The coupling coefficient determines the leakage inductance, which is the working inductance in the circuit. For the proposed CBCL, the leakage inductances of the proposed CBCL are equal to those of the separately designed inductors as derived from the reluctance model in Section IV-B. These leakage inductances are the function of air gap reluctance and can be directly changed by the air gap or number of turns. It has been shown in (14) and (28) that the inductance values of the separately designed inductors are identical to the leakage inductance values of the proposed CBCL, so that the inductance value of the working inductances in the circuit is not affected by joining them. Similarity in (14) and (28) is independent of the coupling coefficient. This is achieved by using the said magnetic core structure of the proposed CBCL. From the design perspective, it is easy to design separate inductors with the required leakage inductance value, and joining them to make the proposed CBCL produces the current balancing performance. Whatever, the coupling coefficient, the leakage inductances will be equal to those of the separate inductors. Due to the physical joining of the separate inductors, the total magnetic volume of the converter does not increase.

E. Current Balancing Operation

The proposed three-winding CBCL balances three currents of the QAB converter as well as generates sufficiently large leakage inductances that can be used for ZVS operation for the active H-bridges. The three separately designed inductors (see Fig. 3) are connected physically to make the proposed CBCL as shown in Fig. 4. The current flowing in the winding generates the flux (ψ_A, ψ_B, ψ_C) in each leg. The black dots in Fig. 4 show the winding direction so that all positive currents entering the winding generate flux in an upward direction on the outer legs. Each flux can be divided into two parts, the balancing fluxes ($\psi_{A,\,m}, \psi_{B,\,m}, \psi_{C,\,m}$) which are responsible for current balancing operation, and the leakage fluxes ($\psi_{A,\,\sigma}, \psi_{B,\,\sigma}, \psi_{C,\,\sigma}$) which are responsible to generate leakage inductances for ZVS operation. The leakage part of the flux escapes from interactions with the other fluxes and, therefore, does not play any role in balancing operation. The balancing part ($\psi_{A,\,m}, \psi_{B,\,m}, \psi_{C,\,m}$) of each generated flux interacts with the balancing part of the other generated fluxes. That part of the flux is equally distributed to the other two legs. The effect of half of each balancing flux is cancelled by the half of the balancing flux generated in another leg, so that all three balancing fluxes cancel the effects of each other. As long as, the three inductor currents $i_{LA}(t)$, $i_{LB}(t)$, and $i_{LC}(t)$ of the active H-bridges A, B, and C are equal to one another, the net magnetic flux $\psi_{\rm net}$ in the core is zero. Due to the mismatch in circuit parameters, an unbalance in the three inductor currents produces a nonzero net magnetic flux in the core. This net flux is responsible for balancing the currents in the windings. Considering the case when two currents become greater than the third one, a nonzero net magnetic flux is generated in the core. According to Lenz's law, this magnetic flux generates the induced electromotive forces that induce voltages across windings in a reverse direction causing to decrease the increased currents and similarly causing to increase the decreased current until all currents become equal and vice versa.

The current balancing performance is dependent on how good is the flux generated in one winding is interacted by the other two windings that is the magnetic coupling between the windings. The relations of the coupling coefficient of the proposed CBCL with the winding currents can be derived from (6) as

$$i_{LA} = k\,(i_{LB} + i_{LC}) \tag{30}$$

$$i_{LB} = k\,(i_{LA} + i_{LC}) \tag{31}$$

$$i_{LC} = k\,(i_{LA} + i_{LB})\,. \tag{32}$$

A higher value of the coupling coefficient means less deviation between the currents, which gives a good current balancing performance. As k approaches 0.5, the three winding currents become equal (i_{LA}= i_{LB}= i_{LC}).

$$\psi_1 = \psi_A = [+(8\mathcal{R}_c + 6\mathcal{R}_g)\,Ni_{LA} - (\mathcal{R}_c + 3\mathcal{R}_g)\,Ni_{LB} - (\mathcal{R}_c + 3\mathcal{R}_g)\,Ni_{LC}] \div [6\mathcal{R}_c\,(\mathcal{R}_c + \mathcal{R}_g)] \tag{21}$$

$$\psi_2 = \psi_B = [-(\mathcal{R}_c + 3\mathcal{R}_g)\,Ni_{LA} + (8\mathcal{R}_c + 6\mathcal{R}_g)\,Ni_{LB} - (\mathcal{R}\mathcal{R}_c + 3\mathcal{R}_g)\,Ni_{LC}] \div [6\mathcal{R}_c\,(\mathcal{R}_c + \mathcal{R}_g)] \tag{22}$$

$$\psi_3 = \psi C = [-(\mathcal{R}_c + 3\mathcal{R}_g)\,Ni_{LA} - (\mathcal{R}_c + 3\mathcal{R}_g)\,Ni_{LB} + (8\mathcal{R}_c + 6\mathcal{R}_g)\,Ni_{LC}] \div [6\mathcal{R}_c\,(\mathcal{R}_c + \mathcal{R}_g)] \tag{23}$$

$$\begin{bmatrix} N\frac{d\psi_A}{dt} \\ N\frac{d\psi_B}{dt} \\ N\frac{d\psi_C}{dt} \end{bmatrix} = \begin{bmatrix} v_A \\ v_B \\ v_C \end{bmatrix} = \begin{bmatrix} \frac{(4\mathcal{R}_c+3\mathcal{R}_g)}{3\mathcal{R}_c(\mathcal{R}_c+\mathcal{R}_g)}N^2 & -\frac{(\mathcal{R}_c+3\mathcal{R}_g)}{6\mathcal{R}_c(\mathcal{R}_c+\mathcal{R}_g)}N^2 & -\frac{(\mathcal{R}_c+3\mathcal{R}_g)}{6\mathcal{R}_c(\mathcal{R}_c+\mathcal{R}_g)}N^2 \\ -\frac{(\mathcal{R}_c+3\mathcal{R}_g)}{6\mathcal{R}_c(\mathcal{R}_c+\mathcal{R}_g)}N^2 & \frac{(4\mathcal{R}_c+3\mathcal{R}_g)}{3\mathcal{R}_c(\mathcal{R}_c+\mathcal{R}_g)}N^2 & -\frac{(\mathcal{R}_c+3\mathcal{R}_g)}{6\mathcal{R}_c(\mathcal{R}_c+\mathcal{R}_g)}N^2 \\ -\frac{(\mathcal{R}_c+3\mathcal{R}_g)}{6\mathcal{R}_c(\mathcal{R}_c+\mathcal{R}_g)}N^2 & -\frac{(\mathcal{R}_c+3\mathcal{R}_g)}{6\mathcal{R}_c(\mathcal{R}_c+\mathcal{R}_g)}N^2 & \frac{(4\mathcal{R}_c+3\mathcal{R}_g)}{3\mathcal{R}_c(\mathcal{R}_c+\mathcal{R}_g)}N^2 \end{bmatrix} \begin{bmatrix} \frac{di_{LA}}{dt} \\ \frac{di_{LB}}{dt} \\ \frac{di_{LC}}{dt} \end{bmatrix} \tag{24}$$

Additionally, the added air gaps in the central legs of the proposed CBCL provide the paths for three leakage magnetic fluxes. Hence, no extra magnetic volume is required for power transfer and ZVS inductors. The proposed CBCL is used for both purposes.

F. Flux Distribution and Core Loss

In both current balanced and unbalanced conditions, the flux in the conventional separate uncoupled inductors remains uniform throughout the magnetic path length of the magnetic core. Whereas, in the proposed CBCL, the flux in the outer legs may be different from the flux in the central legs depending on the current mismatch amplitude. As mentioned previously, the flux generated by each winding of the proposed CBCL (ψ_A, ψ_B, ψ_C) can be divided into two parts, the balancing fluxes ($\psi_{A,\,m}$, $\psi_{B,\,m}$, $\psi_{C,\,m}$), which are responsible for current balancing operation and the leakage fluxes ($\psi_{A,\,\sigma}, \psi_{B,\,\sigma}, \psi_{C,\,\sigma}$), which are responsible to generate leakage inductances for ZVS operation. The leakage part of the flux is escaped from interacting with the other fluxes, therefore, does not play any role in balancing operation. Equations (21) to (23) can be written as

$$\psi_A = \psi_{A,\,m} + \psi_{A,\,\sigma} \tag{33}$$

$$\psi_B = \psi_{B,\,m} + \psi_{B,\,\sigma} \tag{34}$$

$$\psi_C = \psi_{C,\,m} + \psi_{C,\,\sigma}. \tag{35}$$

Because the air gap reluctance is larger than the magnetic core reluctance ($\mathcal{R}_{\rm g} \gg \mathcal{R}_{\rm c}$), the sum of the air gap and magnetic core reluctance can be approximated to the air gap reluctance ($\mathcal{R}_{\rm g} + \mathcal{R}_{\rm c} \cong \mathcal{R}_{\rm g}$). From (21) to (23), the flux components of (33)–(35) can be defined using the said approximation as

$$\psi_{A,\,m} = \frac{\rm N}{6\mathcal{R}_c}\,(6i_{LA} - 3i_{LB} - 3i_{LC}) \tag{36}$$

$$\psi_{B,\,m} = \frac{\rm N}{6\mathcal{R}_c}\,(-3i_{LA} + 6i_{LB} - 3i_{LC}) \tag{37}$$

$$\psi_{C,\,m} = \frac{\rm N}{6\mathcal{R}_c}\,(-3i_{LA} - 3i_{LB} + 6i_{LC}) \tag{38}$$

$$\psi_{A,\,\sigma} = \frac{\rm N}{6\mathcal{R}_{\rm g}}\,(8i_{LA} - i_{LB} - i_{LC}) \tag{39}$$

$$\psi_{B,\,\sigma} = \frac{\rm N}{6\mathcal{R}_{\rm g}}\,(-i_{LA} + 8i_{LB} - i_{LC}) \tag{40}$$

$$\psi_{C,\,\sigma} = \frac{\rm N}{6\mathcal{R}_{\rm g}}\,(-i_{LA} - i_{LB} + 8i_{LC})\,. \tag{41}$$

When the currents are in balanced condition ($i_{LA} = i_{LB} = i_{LC} = i_L$) then $\psi_{A,\,m} = \psi_{B,\,m} = \psi_{C,\,m} = 0$, hence, no balancing flux is linked with the windings. The fluxes linked in this case are only the leakage fluxes as

$$\psi_A = \psi_B = \psi_C = \psi_{A,\,\sigma} = \psi_{B,\,\sigma} = \psi_{C,\,\sigma} = \frac{\rm N}{\mathcal{R}_{\rm g}}\,i_L. \tag{42}$$

Therefore, the total magnetic flux in the central part of the core of the proposed CBCL becomes

$$\psi_A + \psi_B + \psi_C = \psi_{A,\,\sigma} + \psi_{B,\,\sigma} + \psi_{C,\,\sigma} = \frac{\rm N}{\mathcal{R}_{\rm g}}\,3i_L. \tag{43}$$

When the currents are unbalanced, the balancing flux in each outer leg of the proposed CBCL is not zero and is added to the leakage flux algebraically depending on the magnitude of the current mismatch. This results in unequal flux linkage in the windings and has to be accounted for to prevent core saturation in the outer legs of the proposed CBCL. These unequal fluxes are dependent on the weighted differences of the unbalanced currents and can be calculated from (33)–(41) as

$$\psi_A = \frac{\mu_o N A_c}{6}\left[\frac{\mu_r}{l_c}\,(6i_{LA} - 3i_{LB} - 3i_{LC}) + \frac{1}{l_{\rm g}}\,(8i_{LA} - i_{LB} - i_{LC})\right] \tag{44}$$

$$\psi_B = \frac{\mu_o N A_c}{6}\left[\frac{\mu_r}{l_c}\,(-3i_{LA} + 6i_{LB} - 3i_{LC}) + \frac{1}{l_{\rm g}}\,(-i_{LA} + 8i_{LB} - i_{LC})\right] \tag{45}$$

$$\psi_C = \frac{\mu_o N A_c}{6}\left[\frac{\mu_r}{l_c}\,(-3i_{LA} - 3i_{LB} + 6i_{LC}) + \frac{1}{l_{\rm g}}\,(-i_{LA} - i_{LB} + 8i_{LC})\right] \tag{46}$$

where μ_o is the magnetic permeability of free space, N is the number of turns, A_c is the cross-sectional area of the magnetic core, $l_{\rm g}$ is the air gap, and l_c is the magnetic path length of UU-shaped ferrite core. However, while interacting with one another due to strong magnetic coupling between the windings, the balancing fluxes are neutralized ($\psi_{A,\,m} + \psi_{B,\,m} + \psi_{C,\,m} = 0$) in the central part of the core as explained in Section IV-E. The total magnetic flux now in the central part of the core of the proposed CBCL is reduced to leakage flux and given as

$$\psi_A + \psi_B + \psi_C = \psi_{A,\,\sigma} + \psi_{B,\,\sigma} + \psi_{C,\,\sigma} = \frac{\rm N}{\mathcal{R}_{\rm g}}\,(i_{LA} + i_{LB} + i_{LC})\,. \tag{47}$$

The leakage flux per limb of the proposed CBCL is proportional to the average value of currents and is given as

$$\psi_{\,\sigma} = \frac{\rm N}{\mathcal{R}_{\rm g}}\left(\frac{i_{LA} + i_{LB} + i_{LC}}{3}\right). \tag{48}$$

In Fig. 5, the computer simulation of flux distribution in the magnetic core with a mismatch in circuit parameters is presented. When the inductors are uncoupled, Fig. 5(a) and (b) shows the flux in the outer and central legs of the magnetic core, respectively. Fig. 5(c) and (d) shows the flux in the outer and central legs of the proposed CBCL, respectively, when the inductors are coupled. Results from the computer simulation show that flux remains uniform throughout the magnetic path length of the magnetic core for separate uncoupled inductors whereas, after joining the inductors the flux does not remain

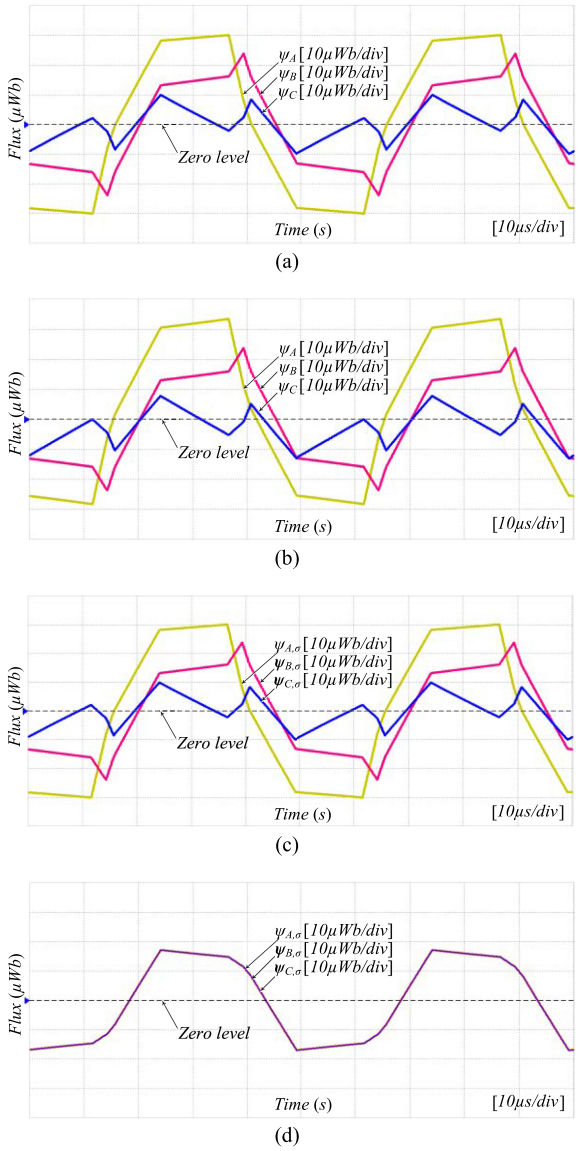

Fig. 5. Computer simulation of flux distribution in the magnetic core with mismatch in the circuit parameters. (a) Flux in the outer legs of separate uncoupled inductors. (b) Flux in the central legs of separate uncoupled inductors. (c) Flux in the outer legs of the proposed CBCL. (d) Flux in the central legs of the proposed CBCL.

uniform throughout the magnetic path length of the magnetic core for the proposed CBCL. The flux in the central legs of the proposed CBCL is reduced to leakage flux due to the cancellation of the balancing flux. Therefore, the core loss in the central legs of the proposed CBCL is also reduced as compared to the case of uncoupled separate inductors.

The outer legs of the proposed CBCL produce the same core loss as the outer legs in the uncoupled separate inductors case. Hence, the proposed CBCL reduces the total core loss compared to separate uncoupled inductors only when there is a mismatch in currents. This reduction in the core loss of the proposed CBCL compared to its uncoupled counterpart is conditional and dependent on the rise in the current mismatch. However, for a balanced current condition, the total core loss of the proposed CBCL remains identical to its uncoupled counterpart.

Fig. 6. (a) Laboratory prototype of the separate uncoupled inductors L_A, L_B, and L_c. (b) Laboratory prototype of the proposed CBCL.

G. Limitations

The proposed CBCL is the result of the magnetic integration of existing ZVS inductors; therefore, it does not change the magnetic volume of a converter. It provides strong magnetic coupling between the windings to effectively balance the currents, addressing a serious problem in the SST industry. It generates sufficient leakage inductances as well. Unfortunately, it does not reduce the size, power density, or cost of a converter. Compared to uncoupled inductors, the core loss of the proposed CBCL is reduced only when there is an increase in the current mismatch. Unbalanced currents in the proposed CBCL result in nonuniform core loss and flux distribution in the core, which may be a concern for proper cooling. Winding with an increased number of turns on each limb of the proposed CBCL may reduce the clearance distance between the windings in the air. Considering the minimum clearance distance for high-voltage applications, the magnetic core of sufficient size should be selected to prevent such shortcomings.

V. Prototype Experiments

In order to validate the performance of the proposed CBCL employed in an asymmetric configuration of a QAB converter, a laboratory prototype for asymmetric configuration of QAB converter along with conventional separate inductors is developed and tested up to 1 kW at 20 kHz. These conventional separate inductors are made using commercially available U-shaped ferrite cores with an air gap in one leg as shown in Fig. 6(a). The inductor design methodology is followed by the area product approach for ac inductor design. The specifications of the magnetic core used in this article are listed in the Appendix. Later, the same inductors are joined physically to make the proposed CBCL as shown in Fig. 6(b). To show the balancing performance, T-structure for the proposed CBCL is considered deliberately and purposefully to create mismatch in magnetics as it can be constructed by easily available U-shaped ferrite cores. Else, "Y" structure would be ideal for the proposed CBCL if the magnetic cores to build a Y-structure were easily available. The converter is tested again using the proposed CBCL and the results are compared with and without the magnetic coupling.

Phase-shift modulation is implemented on a Texas Instruments digital signal processor (DSP) (Delfino TMS320F28335)

TABLE I
CIRCUIT PARAMETERS OF QAB CONVERTER USING CONVENTIONAL SEPARATE INDUCTORS

Test Conditions Using Conventional Separate Inductors				
	Input Side		Output Side	
Phase-shift angles	φ_A	0°	φ_D	90°
	φ_B	20°		
	φ_C	30°		
Conventional inductors	L_A	34.5 µH	L_D	34.2 µH
	L_B	34.7 µH		
	L_C	35 µH		
	N	9 turns		
HF transformer	n_A	9 turns	n_D	9 turns
	n_B	9 turns		
	n_C	9 turns		
DC side voltages	V_{dcA}	100 V	V_{dcD}	120 V
	V_{dcB}	100 V		
	V_{dcC}	77 V		

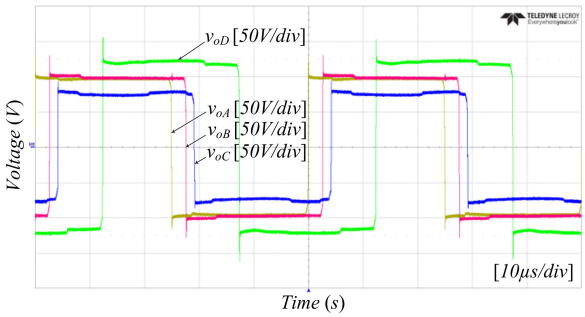

Fig. 7. Experimental voltage waveforms for the ac voltages of active H-bridges of an asymmetrically configured QAB converter using conventional separate inductors with significant mismatch in circuit parameters. $v_{oA(\mathrm{rms})} = 96.3$ V, $v_{oB(\mathrm{rms})} = 98.1$ V, $v_{oC(\mathrm{rms})} = 75.1$ V, $v_{oD(\mathrm{rms})} = 119.5$ V.

to generate rectangular wave voltages on the ac side of the corresponding active H-bridges. The MV side active H-bridges A, B, and C are configured to transfer equal power to the LV side active H-bridge D such that, $v_{oA}(t)$, $v_{oB}(t)$, and $v_{oC}(t)$ are in-phase and are in leading positions from $v_{oD}(t)$. In addition to the natural mismatch in circuit parameters, noticeable mismatches are deliberately created in phases and in the dc side voltages of the active H-bridges.

A. Conventional Structure

Table I shows the circuit parameters of the asymmetric configuration of a QAB converter using conventional separate inductors. The significant mismatches created in the circuit parameters in addition to natural mismatches are highlighted in Table I. Fig. 7 shows the experimental voltage waveforms for the ac side voltages (v_{oA}, v_{oB}, v_{oC}, v_{oD}) of active H-bridges using conventional separate inductors and having a significant mismatch in circuit parameters. The unbalance in three measured currents $i_{LA}(t)$, $i_{LB}(t)$, and $i_{LC}(t)$ can be seen in Fig. 8, which is due to the mismatch in phase as well as mismatch in voltage. The maximum difference in root mean square (rms) values of current is observed equal to 8.9 A.

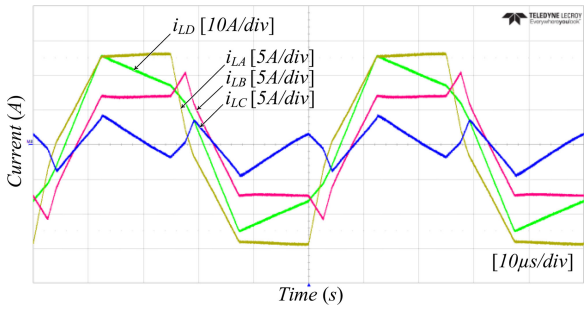

Fig. 8. Experimental current waveforms for the conventional separated inductors employed in an asymmetrically configured QAB converter with significant mismatch in circuit parameters. $i_{LA(\mathrm{rms})} = 11.06$ A, $i_{LB(\mathrm{rms})} = 6.57$ A, $i_{LC(\mathrm{rms})} = 2.13$ A, $i_{LD(\mathrm{rms})} = 17.54$ A.

TABLE II
CIRCUIT PARAMETERS OF QAB CONVERTER USING THE PROPOSED CBCL

Test Conditions Using the Proposed CBCL				
	Input Side		Output Side	
Phase-shift angles	φ_A	0°	φ_D	90°
	φ_B	20°		
	φ_C	30°		
Proposed CBCL	L_{SelfA}	213.6 µH	L_D	34.2 µH
	L_{SelfB}	231.8 µH		
	L_{SelfC}	197.6 µH		
	L_{lkA}	30 µH		
	L_{lkB}	27.6 µH		
	L_{lkC}	25.5 µH		
	k_{AB}	48.5 %		
	k_{BC}	45.0 %		
	k_{CA}	36.9 %		
	N	9 turns		
HF transformer	n_A	9 turns	n_D	9 turns
	n_B	9 turns		
	n_C	9 turns		
DC side voltages	V_{dcA}	100 V	V_{dcD}	120 V
	V_{dcB}	100 V		
	V_{dcC}	77 V		

B. Proposed Structure

Table II shows the circuit parameters used in the asymmetric configuration of a QAB converter using the proposed three-winding CBCL instead of conventional separate inductors. It can be seen from the experimental results given in Fig. 9 that, with the same significant mismatch in circuit parameters as applied for the conventional method, the proposed CBCL balances three currents almost perfectly. The maximum difference in rms values of current is reduced to 1.1 A. Hence, the geometrical tolerances and asymmetries due to nonsymmetric structure of the magnetic core, and nonidentical self and leakage inductances of the proposed CBCL do not affect the balancing performance. Experimental waveforms for ZVS operation in all 16 switches are shown in Figs. 10 and 11.

C. Step-Input Response Using the Proposed CBCL

To validate the dynamic performance of the proposed CBCL, a step-input response in an open-loop is captured in Fig. 12. The

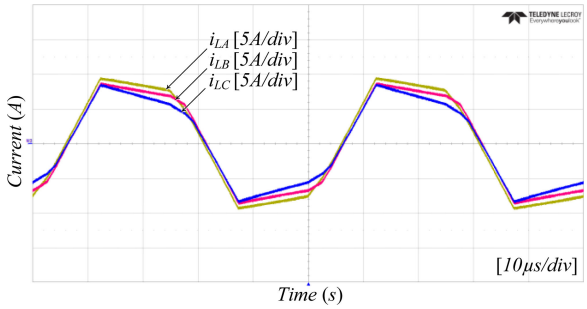

Fig. 9. Experimental current waveforms of the proposed CBCL in an asymmetric configuration of QAB converter with significant mismatch in circuit parameters. $i_{LA(\mathrm{rms})} = 7.00$ A, $i_{LB(\mathrm{rms})} = 6.45$ A, $i_{LC(\mathrm{rms})} = 5.90$ A.

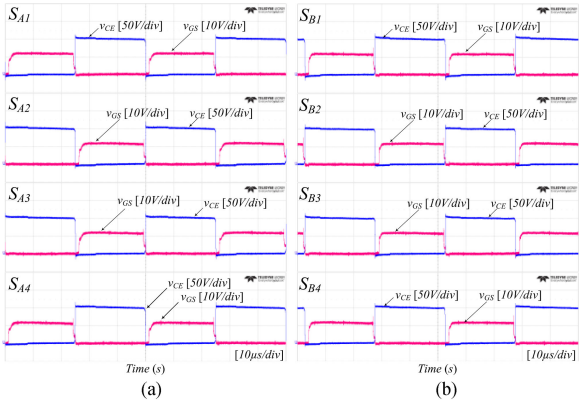

Fig. 10. Experimental waveforms of gate signals and voltage across the switch using the proposed CBCL in an asymmetrically configured QAB converter showing ZVS with significant mismatch in circuit parameters. (a) Active H-bridge A. (b) Active H-bridge B.

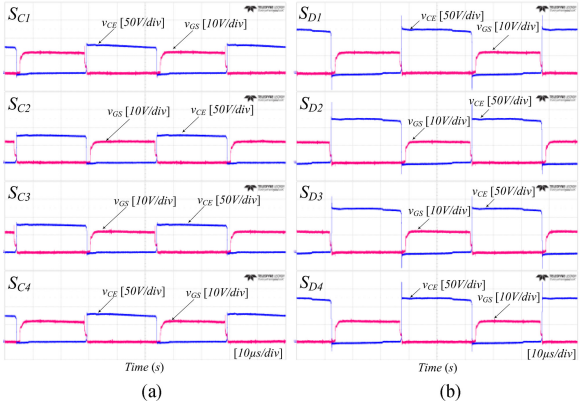

Fig. 11. Experimental waveforms of gate signals and voltage across the switch using the proposed CBCL in an asymmetrically configured QAB converter showing ZVS with significant mismatch in circuit parameters. (a) Active H-bridge C. (b) Active H-bridge D.

step in all input dc side voltages is applied simultaneously from zero to 100 V. The magnified waveforms of current in Fig. 12(b) show that during the transition with a significant mismatch in circuit parameters, the proposed CBCL still balances the currents perfectly.

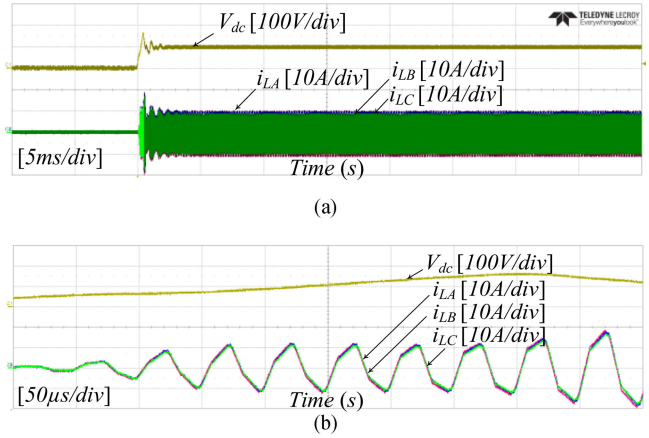

Fig. 12. (a) Step-input response of the proposed CBCL in an asymmetrically configured QAB converter with significant mismatch in circuit parameters. (b) Magnified zoom waveforms during transition.

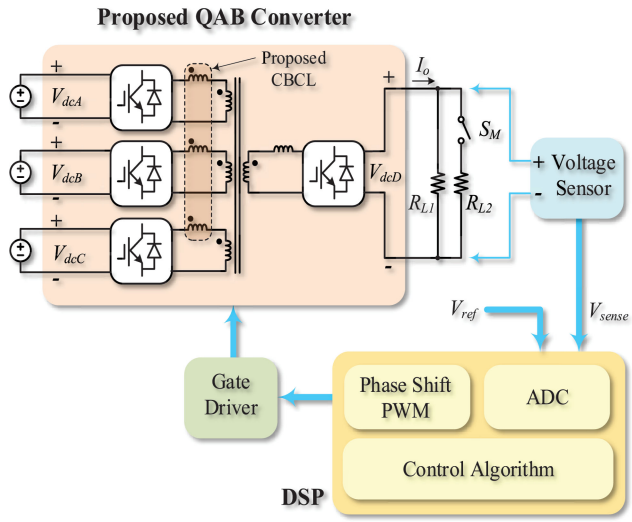

Fig. 13. Block diagram of control strategy to observe the step-load response of asymmetrically configured QAB converter using the proposed CBCL with significant mismatch in circuit parameters.

D. Step-Load Response Using the Proposed CBCL

The output of the QAB converter behaves like a current source and is a function of phase difference. To apply a step-load change at the output and to observe the behavior of the proposed CBCL, the output voltage needs to be controlled in a closed-loop. For this purpose, the control strategy shown in Fig. 13 is implemented using DSP. The behavior of the proposed CBCL with a significant mismatch in circuit parameters is observed by applying the step-load change from 6 to 12 A at a reference of 60 V as presented in Figs. 14 and 15. Fig. 14 shows the normal and magnified current (i_{LA}, i_{LB}, i_{LC}) waveforms before and after applying step-load. Whereas, Fig. 15 shows the normal and magnified voltage (v_{oA}, v_{oB}, v_{oD}) waveforms at before and after applying step-load. The magnified waveforms of current before and after applying step-load reveal that the current balancing

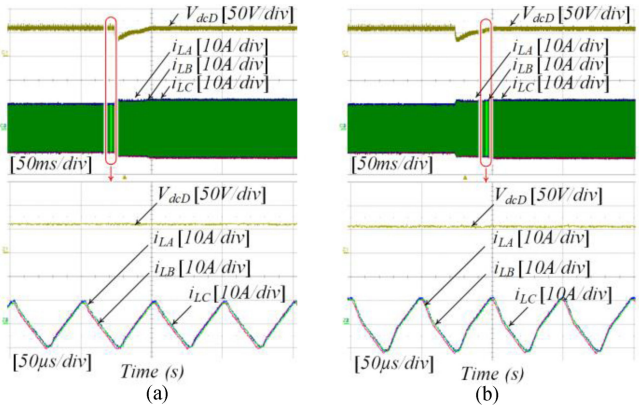

Fig. 14. Step-load response using the proposed CBCL in an asymmetrically configured QAB converter with significant mismatch in circuit parameters. Magnified current waveforms (a) before applying step-load and (b) after applying step-load.

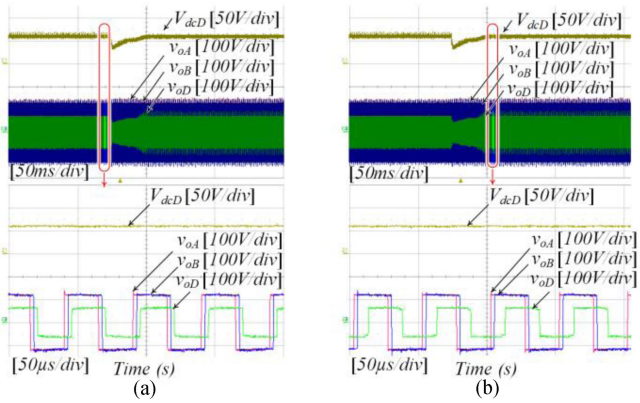

Fig. 15. Step-load response using the proposed CBCL in an asymmetrically configured QAB converter with significant mismatch in circuit parameters. Magnified voltage waveforms (a) before applying step-load and (b) after applying step-load. (c) Step-input response using the proposed CBCL.

performance of the proposed CBCL is not affected by step-load. It automatically balances the three currents effectively without any dedicated balancing controller.

VI. Conclusion

In this article, a CBCL-based asymmetric configuration of a QAB converter is proposed. When transferring equal power from MV to LV side with very significant mismatches, the proposed CBCL effectively balances the current among three active H-bridges without a dedicated controller and expensive sensors, and it offers sufficient inductances for ZVS operation as well. Furthermore, the proposed CBCL does not increase the overall magnetic volume of a converter because it is made by using the magnetics of the already present inductors required for power transfer and ZVS operation in a converter. The magnetic structure makes the design simple and intuitive. The performance of the proposed CBCL has been verified through experimental work.

Appendix

The specifications of the U-shaped ferrite core with an air gap in one leg used in this article are as follows:

Manufacturer	TODA-ISU
Material	Ferrite FM4
Core cross-sectional area	334 mm^2
Magnetic path length (UU-shaped)	160 mm
Inductance factor (UU-shaped)	5.1 μH
Air gap in one leg (U-shaped)	1 mm
Total air gap (UU-shaped)	2 mm

References

[1] X. She, A. Q. Huang, and R. Burgos, "Review of solid-state transformer technologies and their application in power distribution systems," *IEEE J. Emerg. Sel. Topics Power Electron.*, vol. 1, no. 3, pp. 186–198, Sep. 2013.

[2] L. F. Costa, G. Buticchi, and M. Liserre, "Quad-active-bridge DC–DC converter as cross-link for medium-voltage modular inverters," *IEEE Trans. Ind. Appl.*, vol. 53, no. 2, pp. 1243–1253, Mar./Apr. 2017.

[3] L. F. Costa, G. De Carne, G. Buticchi, and M. Liserre, "The smart transformer: A solid-state transformer tailored to provide ancillary services to the distribution grid," *IEEE Power Electron. Mag.*, vol. 4, no. 2, pp. 56–67, Jun. 2017.

[4] L. F. Costa, F. Hoffmann, G. Buticchi, and M. Liserre, "Comparative analysis of multiple active bridge converters configurations in modular smart transformer," *IEEE Trans. Ind. Electron.*, vol. 66, no. 1, pp. 191–202, Jan. 2019.

[5] A. Chub, L. Costa, and M. Liserre, "Analysis and design of asymmetric quad-active-bridge converter," in *Proc. 43rd Annu. Conf. IEEE Ind. Electron. Soc.*, 2017, pp. 5367–5372.

[6] M. Liserre, M. Andresen, L. Costa, and G. Buticchi, "Power routing in modular smart transformers: Active thermal control through uneven loading of cells," *IEEE Ind. Electron. Mag.*, vol. 10, no. 3, pp. 43–53, Sep. 2016.

[7] M. Liserre, G. Buticchi, M. Andresen, G. De Carne, L. F. Costa, and Z. Zou, "The smart transformer: Impact on the electric grid and technology challenges," *IEEE Ind. Electron. Mag.*, vol. 10, no. 2, pp. 46–58, Jun. 2016.

[8] L. F. Costa, G. Buticchi, and M. Liserre, "Optimum design of a multiple-active-bridge DC–DC converter for smart transformer," *IEEE Trans. Power Electron.*, vol. 33, no. 12, pp. 10112–10121, Dec. 2018.

[9] N. Hur and K. Nam, "A robust load-sharing control scheme for parallel-connected multisystems," *IEEE Trans. Ind. Electron.*, vol. 47, no. 4, pp. 871–879, Aug. 2000.

[10] P. Karlsson and J. Svensson, "DC bus voltage control for a distributed power system," *IEEE Trans. Power Electron.*, vol. 18, no. 6, pp. 1405–1412, Nov. 2003.

[11] G. Buticchi, M. Andresen, M. Wutti, and M. Liserre, "Lifetime-based power routing of a quadruple active bridge DC/DC converter," *IEEE Trans. Power Electron.*, vol. 32, no. 11, pp. 8892–8903, Nov. 2017.

[12] T. Zhao, G. Wang, S. Bhattacharya, and A. Q. Huang, "Voltage and power balance control for a cascaded H-Bridge converter-based solid-state transformer," *IEEE Trans. Power Electron.*, vol. 28, no. 4, pp. 1523–1532, Apr. 2013.

[13] S. Falcones, R. Ayyanar, and X. Mao, "A DC–DC multiport-converter-based solid-state transformer integrating distributed generation and storage," *IEEE Trans. Power Electron.*, vol. 28, no. 5, pp. 2192–2203, May 2013.

[14] Y. Nakakohara, H. Otake, T. M. Evans, T. Yoshida, M. Tsuruya, and K. Nakahara, "Three-phase LLC series resonant DC/DC converter using SiC MOSFETs to realize high-voltage and high-frequency operation," *IEEE Trans. Ind. Electron.*, vol. 63, no. 4, pp. 2103–2110, Apr. 2016.

[15] C. Liu *et al.*, "Magnetic-coupling current-balancing cells based input-parallel output-parallel LLC resonant converter modules for high-frequency isolation of DC distribution systems," *IEEE Trans. Power Electron.*, vol. 31, no. 10, pp. 6968–6979, Oct. 2016.

[16] J. Liu, C. Li, Z. Zheng, K. Wang, and Y. Li, "Current discrepancy mitigation of input-parallel output-parallel dual active bridge converters using coupled inductors," *IEEE Trans. Ind. Electron.*, doi: 10.1109/TIE.2020.3013793.

[17] Y. Dou, Z. Ouyang, and M. A. E. Andersen, "Integrated coupled inductors with functionality of current balancing transformer for two-phase synchronous DC–DC converters," *IEEE Trans. Power Electron.*, vol. 35, no. 5, pp. 4472–4476, May 2020.
[18] M. Noah *et al.*, "A current sharing method utilizing single balancing transformer for a multiphase LLC resonant converter with integrated magnetics," *IEEE J. Emerg. Sel. Topics Power Electron.*, vol. 6, no. 2, pp. 977–992, Jun. 2018.
[19] Z. Zhang, J. Huang, and Y. Xiao, "GaN-based 1-MHz partial parallel dual active bridge converter with integrated magnetics," *IEEE Trans. Ind. Electron.*, vol. 68, no. 8, pp. 6729–6738, Aug. 2021.
[20] U. Ahmad, H. Cha, and N. Naseem, "Integrated current balancing transformer based input-parallel output-parallel LLC resonant converter modules," *IEEE Trans. P ower E lectron.*, vol. 36, no. 5, pp. 5278–5289, May 2021.
[21] N. Naseem, H. Cha, and J. Kim, "Current balancing technique in symmetrical configuration of quad-active-bridge converter using integrated magnetic current balancing cells," in *Proc. IEEE Energy Convers. Congr. Expo.*, 2019, pp. 1353–1358.
[22] N. Naseem, H. Cha, U. Ahmad, and H. Kim, "Quad-active-bridge converter with integrated magnetic current balancing cell for DC distribution system," in *Proc. 10th Int. Conf. Power Electron.*, 2019, pp. 2653–2659.

Nabeel Naseem (Student Member, IEEE) was born in Pakistan. He received the M.Sc. degree in applied physics (specialization in electronics) from the University of Karachi, Karachi, Pakistan. He is currently working toward the combined M.S. and Ph.D. degree in energy engineering with the School of Energy Engineering, Kyungpook National University, Daegu, South Korea.

His research interests include design, manufacturing, and control techniques for efficient power electronic converter systems, high-frequency magnetic design, and components and their use in a wide range of applications.

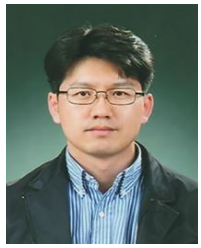

Honnyong Cha (Senior Member, IEEE) received the B.S. and M.S. degrees in electronics engineering from Kyungpook National University, Daegu, South Korea, in 1999 and 2001, respectively, and the Ph.D. degree in electrical engineering from Michigan State University, East Lansing, MI, USA, in 2009.

From 2001 to 2003, he was a Research Engineer with the Power System Technology Company, Ansan, South Korea. From 2010 to 2011, he was a Senior Researcher with the Korea Electrotechnology Research Institute, Changwon, South Korea. In 2011, he joined the School of Energy Engineering, Kyungpook National University. In 2017, he was a Visiting Scholar with the Future Energy Electronics Center, Virginia Polytechnic Institute and State University, Blacksburg, VA, USA. His research interests include high-power dc–dc converters, dc–ac inverters, Z-source inverters, and power conversion for electric vehicles and wind power generation.